

ASYMPTOTIC SOLUTIONS FOR BACKSCATTERING BY SMOOTH 2D SURFACES

I. M. Fuks

Zel Technologies, LLC
and NOAA/Environmental Technology Laboratory
R/ET-0, 325 Broadway, Boulder, CO 80305, USA

Abstract—High-frequency asymptotic expansions of electric and magnetic fields are obtained at a perfectly conducting smooth 2-D surface illuminated by a plane incident wave in two cases of *TE* and *TM* linear polarization. Diffraction corrections up to the second order of the inverse large parameter $p = ak$ (where a is a curvature radius at the specularly reflected point, and k is a field wavenumber) to the geometrical optics fields, and specifically to their phases, backscattering cross-sections (*HH* and *VV* for *TE* and *TM* polarizations, correspondingly), as well as the polarization ratio *HH/VV*, are derived for the specular points of a general form. These general results are applied to backscattering from cylinders with conical section directrices (circle, parabola, ellipse and hyperbola), and a number of new compact explicit equations are derived, especially for elliptic and hyperbolic cylinders illuminated at an arbitrary incidence angle relative to their axes of symmetry.

1 Introduction

2 Asymptotic Expansions for the Wave Fields at a Perfectly Conducting Surface

3 Backscattered Fields in the Far Zone

- 3.1 Phase Corrections
- 3.2 Backscattering Cross-Sections
- 3.3 Polarization Ratio
- 3.4 Dependence on the Angle of Incidence

4 Asymptotic Expansions for Fields Backscattered from a Cylinder with a Conic Section Directrix

- 4.1 The Circular Cylinder

- 4.2 The Parabolic Cylinder
- 4.3 The Elliptic Cylinder
- 4.4 The Hyperbolic Cylinder

5 Conclusions

Acknowledgment

References

1. INTRODUCTION

The high-frequency asymptotic of electromagnetic fields backscattered by a smooth body with an arbitrary shape is of great interest for many physical problems and engineering applications. The progress in numerical methods applications to the diffraction problem does not diminish the actuality of obtaining the high-frequency asymptotic expansions in the analytical form: the higher the frequency, the more discretization points are needed, and the cost of computing is increasing catastrophically. The analytical results for the high-frequency limit play a valuable role as tests for existing and developing computer codes.

For a simply shaped body, such as a circular or parabolic cylinder, sphere or ellipsoid, when the separation of variables in the Helmholtz equation is possible, the exact solution of the diffraction problem can be represented as an expansion on the infinite series of eigen functions of the Helmholtz equation (see, e.g., [1]). Even in these simplest cases, obtaining the expansion of the diffracted field in a series of reversed powers of wave frequency ω is not a trivial problem, because of a drastic increase in the number of terms in these series which have to be taken into account. The advanced methods of complex analysis (the so-called “Watson transformation” [2] or its modifications [3, 4]) can be employed to obtain the high-frequency asymptotic expansions in these cases. However, the number of body shapes for which the exact solutions are known is limited only by a few cases (see, e.g., [5]), and in a general case, only some approximative methods can be used for this problem solving.

One of the most powerful methods of an asymptotic solution of the general diffraction problem was suggested and developed in the set of fundamental papers ([6] and [7] and references therein). This approach later evolved in numerous works and was generalized for solving many other diffraction problems. Over time, it was designated as a Ray Method [8], and now it underlies the Geometrical Theory of Diffraction (see [9, 10] and bibliographies therein). In the framework of this

method, the asymptotic solution of the diffraction problem is obtained in two steps. The first step is the solution of the eikonal equation, which gives the geometrical optics solution of the problem, i.e., the shape of the reflected wave phase fronts, and the ray congruence as the set of normals to them. The amplitude and the phase of the diffracted wave can be found in the second step by solving the set of so-called, “transport equations” for the coefficients of expansion of the solution in an asymptotic series of reversed powers of the wave frequency ω . The first coefficient corresponds to the geometrical optics (GO) result: the phase of the reflected wave is equal to the length of the optical path along the corresponding ray, and the amplitude of the scattered wave is proportional to the square root of the wave front Gaussian curvature, which guarantees the energy conservation inside every infinitesimal ray tube. The high-order terms take into account the phenomenon of the “transverse diffusion” of the wave field at the surfaces of wave fronts (i.e., in directions perpendicular to the rays): they can be obtained from the set of recursive equations by integrating the derivatives of the eikonal along the rays. This solution can be represented in a general form for an arbitrarily shaped 2-D and 3-D body for all possible specific cases of a diffraction problem: for the incident wave with an arbitrary wavefront (plane, cylindrical, spherical, etc.); at every spatial point located at the arbitrary distance along the corresponding ray, including observation points in the shadow (in this case, so-called “diffraction rays” replace the GO rays); for scattering in different directions (including, in particular, the backscattering), etc. In principle, having the set of the recursive equations, it is possible to obtain the coefficients of terms $\sim 1/\omega^n$ of any order of n .

On the other hand, the wide generality of the Ray Method has some disadvantages: the coefficients of the field asymptotic expansion are represented as a quadratures of spatial derivatives of an eikonal, which is assumed to be found in the first step of the problem solving, i.e., in the GO limit. Despite the fact that the solution of the last problem was obtained in [11] for reflection of the arbitrarily shaped incident wave front by the specular point of a general form (see also [12–14], and references in [15], section 28), the resulting equations obtained are so cumbersome that it is impossible to perform the next steps to obtain any result beyond the GO limit, i.e., to perform the analytical integration along the ray of the eikonal derivatives in a general case, even for the first corrections $\sim 1/\omega$ to the GO formulae. (Note that to obtain the diffraction corrections to the phase of the reflected wave, it is necessary to obtain terms of the order $\sim 1/\omega$, and to the amplitude – of the order $\sim 1/\omega^2$). Apparently, this fact is the reason that the applicability of the Ray Method for solving the wave scattering problem

(in the light zone, where at least one specular point exists) even for the 2-D case was demonstrated in [6] only for the circular and parabolic cylinder (with the incidence along the parabola axis only). In these cases the set of rays has the simplest form, and the full set of recursive equations for all coefficients of the wave field asymptotic expansion can be obtained in an explicit form. In a 3-D case the explicit equations were obtained also only for the simplest shaped bodies. In the case of arbitrarily shaped bodies, only the first correction ($\sim 1/\omega$) to the GO result of diffraction by a body of revolution was obtained in [16]. It has such a cumbersome appearance (see also Eq. (I.122) at page 28 in [5]) that the next coefficient for the term of order of $\sim 1/\omega^2$ was not obtained up to now. Moreover, it has taken 20 years (see [17]) to discover some errors in [16], where this result was first published.

In [18], we obtained the explicit expressions for the first two corrections ($\sim 1/\omega$ and $\sim 1/\omega^2$) to the GO solution in the far zone for the wave field, backscattered from a single specular point at the smooth, perfectly conducting 2-D body of an arbitrary shape. The fields and their normal derivatives at the surface were obtained with an accuracy of $1/\omega^2$ by iteration of the corresponding surface integral equations for *TE* and *TM* incident waves. The backscattered fields in the far zone were found as an asymptotic expansion of the Huygens-Kirchhoff integral with the same accuracy of $1/\omega^2$. The advantage of the obtained results over the Ray Method equations is that the final formulae in [18] contain in the explicit form the derivatives of the surface profile at the specular point (up to the sixth order), but not the derivatives of the eikonal. As distinct from the classical Ray Method, which gives the result in the most general form, these equations are obtained only for the specific case of a plane wave backscattering from the single specular point (line at the 2-D surface) in the far zone, where there are no caustics and the scattered wave have a cylindrical divergency.

In this paper, we employ the equations derived in [18] to obtain the high-frequency asymptotic expansions of EM fields backscattered by the cylindrical surfaces having a conic section directrix (circle, ellipse, parabola and hyperbola). Corrections of $\sim 1/\omega^2$ to the GO formulae are obtained for two polarizations of the incident field as functions of the angle of incidence. These equations greatly expand upon the number of analytical expressions that can be found in the reference book [5]. These corrections also can play a significant role in comparing the numerically calculated cross-sections in [19] with the analytical results for a smooth 2-D surface with known differential parameters.

The paper is organized as follows. In Section 2, the high-frequency expansion of *TE* and *TM* fields at the surface are obtained up to

the terms on the order of $\sim 1/k^2$ by two consecutive iterations of the corresponding integral equations. These expansions are used in Section 3 for deriving the far-zone backscattered fields, using the Huygens-Kirchhoff principle. In Section 4, the general results derived above are applied to the cylinders with a conic section directrix, and explicit equations for phase and backscattering cross-sections are obtained and analyzed. In the Conclusions, a summation of the most significant results is presented.

2. ASYMPTOTIC EXPANSIONS FOR THE WAVE FIELDS AT A PERFECTLY CONDUCTING SURFACE

Hereinafter we consider scattering of the monochromatic wave of frequency ω , and the phase factor $\exp(-i\omega t)$ is omitted. In the geometrical optics limit, backscattering (retroreflection) from a smooth surface S is caused only by the specular points, where the direction \mathbf{N} of normal-to-the-surface S is opposite to the direction of the wave vector $\mathbf{k} = k\boldsymbol{\alpha}_0$ of the incident wave $\sim \exp(i\mathbf{k}\mathbf{R})$, where $k = \omega/c$ is the wave number, c is a wave propagation velocity, and $\boldsymbol{\alpha}_0$ is the unit vector of the propagation direction of the incident plane wave. For a 2-D surface, without a loss of generality, we can specify the equation of the surface S in the form $z = Z(x)$, with the origin of the Cartesian coordinates (x, y, z) in the specular point O , the axis Oz directed along the normal \mathbf{N} , and the axis Oy directed along the surface S directrix (Fig. 1).

The arbitrary polarized incident wave can be represented as a

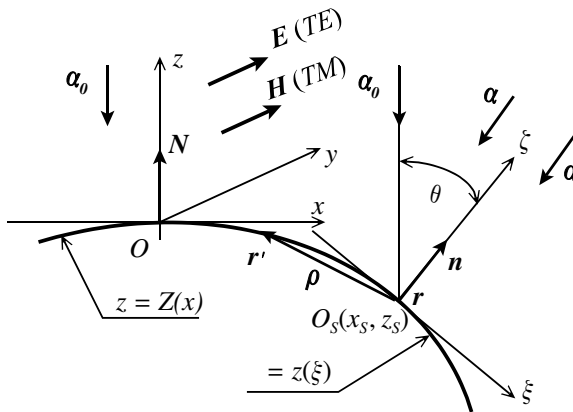


Figure 1. The frames of reference related to the specular reflecting point O at normal incidence and to O_S at inclined incidence.

linear superposition of two eigenwaves: the *TE* wave with the electric field vector $\mathbf{E}_0 = (0, E_0, 0)$ directed along the surface generatrix *Oy*, and the *TM* wave with the magnetic field vector $\mathbf{H}_0 = (0, H_0, 0)$. For a perfectly conducting surface *S* and for these two cases of polarization, the *scattered* fields $\mathbf{E}_{sc} = (0, E_{sc}, 0)$ and $\mathbf{H}_{sc} = (0, H_{sc}, 0)$ in an arbitrary point \mathbf{R} can be represented as surface integrals, according to the Huygens-Kirchhoff principle:

$$E_{sc}(\mathbf{R}) = - \int_S \frac{\partial E(\mathbf{r})}{\partial n} G_0(\mathbf{R}, \mathbf{r}) d\mathbf{r}, \quad (1)$$

$$H_{sc}(\mathbf{R}) = \int_S H(\mathbf{r}) \frac{\partial}{\partial n} G_0(\mathbf{R}, \mathbf{r}) d\mathbf{r}, \quad (2)$$

where $G_0(\mathbf{R}, \mathbf{r})$ is the Green function of the Helmholtz equation for a free space

$$G_0(\mathbf{R}, \mathbf{r}) = \frac{1}{4\pi |\mathbf{R} - \mathbf{r}|} e^{ik|\mathbf{R} - \mathbf{r}|}, \quad (3)$$

and $\partial/\partial n$ implies the derivative along the normal \mathbf{n} to the surface *S* at the point of integration $\mathbf{r} \in S$ (see Fig. 1). The *total* magnetic field $H(\mathbf{r})$ and the normal derivative $\partial E(\mathbf{r})/\partial n$ of the *total* electrical field $E(\mathbf{r})$ at surface *S*, in turn, are the solutions of the corresponding integral equations:

$$\frac{\partial E(\mathbf{r})}{\partial n} = 2 \frac{\partial E_0(\mathbf{r})}{\partial n} - 2 \int_S \frac{\partial E(\mathbf{r}')}{\partial n'} \frac{\partial}{\partial n} G_0(\mathbf{r}, \mathbf{r}') d\mathbf{r}', \quad (4)$$

$$H(\mathbf{r}) = 2H_0(\mathbf{r}) + 2 \int_S H(\mathbf{r}') \frac{\partial}{\partial n'} G_0(\mathbf{r}, \mathbf{r}') d\mathbf{r}'. \quad (5)$$

These two equations are entirely equivalent to the integral equations for sound-wave pressure at free and perfectly rigid surfaces, correspondingly.

Instead of $\partial E(\mathbf{r})/\partial n$ and $H(\mathbf{r})$, let us introduce two new functions u_e and u_h :

$$H(\mathbf{r}) = u_h(\mathbf{r}) e^{i\mathbf{k}\mathbf{r}}, \quad (6)$$

$$\frac{\partial E(\mathbf{r})}{\partial n} = i(\mathbf{k} \cdot \mathbf{n}) u_e(\mathbf{r}) e^{i\mathbf{k}\mathbf{r}}, \quad (7)$$

and the new variable of integration $\boldsymbol{\rho} = \mathbf{r}' - \mathbf{r}$ in (4) and (5). Assuming that the incident waves $\mathbf{E}_0(\mathbf{r})$ and $\mathbf{H}_0(\mathbf{r})$ have the unit amplitudes, i.e., $\mathbf{E}_0(\mathbf{r}) = \mathbf{e}_y \exp(i\mathbf{k}\mathbf{r})$ for *TE* waves and $\mathbf{H}_0(\mathbf{r}) = \mathbf{e}_y \exp(i\mathbf{k}\mathbf{r})$ for *TM* waves, where \mathbf{e}_y is a unit vector along the *Oy* axis and $k_y = 0$, we

obtain instead of (4) and (5):

$$u_e(\mathbf{r}) = 2 + \frac{1}{2\pi} \int_S u_e(\mathbf{r} + \boldsymbol{\rho}) \frac{\boldsymbol{\rho} \cdot \mathbf{n} \boldsymbol{\alpha}_0 \cdot \mathbf{n}'}{\rho^3 \boldsymbol{\alpha}_0 \cdot \mathbf{n}} (ik\rho - 1) e^{ik(\rho + \boldsymbol{\rho} \cdot \boldsymbol{\alpha}_0)} d\boldsymbol{\rho}, \quad (8)$$

$$u_h(\mathbf{r}) = 2 + \frac{1}{2\pi} \int_S u_h(\mathbf{r} + \boldsymbol{\rho}) \frac{\boldsymbol{\rho} \cdot \mathbf{n}'}{\rho^3} (ik\rho - 1) e^{ik(\rho + \boldsymbol{\rho} \cdot \boldsymbol{\alpha}_0)} d\boldsymbol{\rho}, \quad (9)$$

where $\mathbf{n} = \mathbf{n}(\mathbf{r})$ and $\mathbf{n}' = \mathbf{n}(\mathbf{r} + \boldsymbol{\rho})$. In the high-frequency limiting case $k \rightarrow \infty$, integral terms in these equations turn to zero, which corresponds to the tangent plane approximation (or Kirchhoff method, see [20, 21]): at a perfectly conducting surface, the tangent component of the magnetic field and the normal derivative of the tangent component of the electric field are doubled, i.e., $u_e(\mathbf{r}) = u_h(\mathbf{r}) = 2$, as it occurs at reflection from the perfect plane tangent to the curved surface S at every point $\mathbf{r} \in S$. Our goal is to find the corrections to these solutions, caused by the diffraction effects at the curved surface.

At every point $\mathbf{r} \in S$ (see Fig. 1), let us introduce the local Cartesian frame of reference (ξ, η, ζ) , with axis $O_S\zeta$ directed along the normal \mathbf{n} , axis $O_S\eta$ directed along Oy , and, consequently, axis $O_S\xi$ is the tangent to the surface S on the plane (x, O, z) . Let us set the equation of the surface in this reference frame in the form $\zeta = z(\xi)$; vector $\boldsymbol{\rho}$ has the following components $\boldsymbol{\rho} = (\xi, \eta, z(\xi))$, and the unit vector \mathbf{n}' takes the form:

$$\mathbf{n}' = \mathbf{n}(\mathbf{r} + \boldsymbol{\rho}) = \frac{\mathbf{e}_\zeta - \gamma}{\sqrt{1 + \gamma^2}}, \quad (10)$$

where $\gamma = (dz/d\xi, 0, 0)$ is the surface slope at the point $\mathbf{r}' = \mathbf{r} + \boldsymbol{\rho}$. Change from integration over $d\boldsymbol{\rho}$ in (8) and (9) to integration over the plane $\boldsymbol{\rho}_\perp = (\xi, \eta)$ tangent to the surface S at point \mathbf{r} , using the relations:

$$d\boldsymbol{\rho} = \frac{d\boldsymbol{\rho}_\perp}{n_\zeta(\mathbf{r} + \boldsymbol{\rho})}, \quad d\boldsymbol{\rho}_\perp = d\xi d\eta, \quad n_\zeta(\mathbf{r} + \boldsymbol{\rho}) = \frac{1}{\sqrt{1 + \gamma^2}}. \quad (11)$$

Taking into account $\rho = \sqrt{\rho_\perp^2 + z^2(\xi)}$, and expanding the kernels of the integral equations (8) and (9) in series of $z(\xi)$ up to its second power, we can represent (8) and (9) in the form:

$$u_e(\mathbf{r}) = 2 + \frac{1}{2\pi} \iint_{-\infty}^{\infty} u_e(\mathbf{r} + \boldsymbol{\rho}) \frac{ik\rho_\perp - 1}{\rho_\perp^3} z(\xi) \times \left[1 - ik \cos \theta z(\xi) + \tan \theta \frac{dz(\xi)}{d\xi} \right] e^{ik\rho_\perp(1 + \sin \theta \cos \varphi)} d\xi d\eta, \quad (12)$$

$$u_h(\mathbf{r}) = 2 + \frac{1}{2\pi} \iint_{-\infty}^{\infty} u_h(\mathbf{r} + \boldsymbol{\rho}) \frac{ik\rho_{\perp} - 1}{\rho_{\perp}^3} \left[z(\xi) - \xi \frac{dz(\xi)}{d\xi} \right] \times \\ [1 - ik \cos \theta z(\xi)] e^{ik\rho_{\perp}(1 + \sin \theta \cos \varphi)} d\xi d\eta, \quad (13)$$

where $\rho_{\perp} = \sqrt{\xi^2 + \eta^2}$, and θ is the local incident angle at $\mathbf{r} \in S$, i.e., $\boldsymbol{\alpha}_0 \cdot \mathbf{n} = -\cos \theta$, and φ is the azimuthal angle between the direction of vector $\boldsymbol{\rho}_{\perp}$ and axis $OS\xi$, i.e., $\xi = \rho_{\perp} \cos \varphi$, $\eta = \rho_{\perp} \sin \varphi$. Here, we take into account that in a high-frequency limit, for a large but finite value of k , only the small vicinity of the point \mathbf{r} is essential for integration in (12) and (13), where function $z(\xi)$ can be represented as a series expansion in powers of ξ , and the limits of integration can be expanded to infinity, if the linear dimension of the scattered body essentially exceeds the Fresnel zone $\sqrt{\lambda a}$, where $\lambda = 2\pi/k$ is a wavelength, and a is a local curvature radius of the surface directrix at the point \mathbf{r} . For obtaining the diffraction corrections up to the terms of order k^{-2} , it is sufficient to consider only the first two non-vanishing terms of this expansion:

$$z(\xi) = -\frac{\xi^2}{2a} - \frac{\xi^3}{3b} + \dots \quad (14)$$

Here, we take into account that $dz(\xi)/d\xi = 0$ at $\xi = 0$. Substituting (14) into (12) and (13), and introducing the dimensionless variables $\mathbf{p} = k\mathbf{r}$ and $\mathbf{t} = k\boldsymbol{\rho}_{\perp}$ instead of \mathbf{r} and $\boldsymbol{\rho}_{\perp}$, we can represent (12), and (13) in the form:

$$u_{e,h}(\mathbf{p}) = 2 \mp \int_0^{\infty} dt \int_0^{2\pi} [Y_1(t, \varphi) + Y_{e,h}(t, \varphi)] u_{e,h}(\mathbf{p} + \mathbf{t}) d\varphi, \quad (15)$$

where the upper sign relates to $u_e(\mathbf{p})$ and the lower one to $u_h(\mathbf{p})$, and kernels $Y_1, Y_{e,h}$ have the form:

$$Y_1(t, \varphi) = \frac{(it - 1) \cos^2 \varphi}{4\pi ak} e^{it(1 + \sin \theta \cos \varphi)}, \quad (16)$$

$$Y_e(t, \varphi) = t \cos \varphi \left(\frac{2a}{3bk} - \frac{\tan \theta}{ak} + it \cos \varphi \frac{\cos \theta}{2ak} \right) Y_1(t, \varphi), \quad (17)$$

$$Y_h(t, \varphi) = t \cos \varphi \left(\frac{4a}{3bk} + it \cos \varphi \frac{\cos \theta}{2ak} \right) Y_1(t, \varphi). \quad (18)$$

We will seek the solutions of (15) in the form of an iteration series in powers of $1/k$:

$$u_{e,h} = u_{e,h}^{(0)} + u_{e,h}^{(1)} + u_{e,h}^{(2)} + \dots, \quad (19)$$

where $u_{e,h}^{(n)} \sim 1/k^n$ and $u_{e,h}^{(0)} = 2$. The first two iterations in (15) give the following explicit expansion for the surface values of $u_{e,h}$:

$$u_{e,h}(\mathbf{r}) = 2 \left\{ 1 \pm \frac{i}{2ak \cos^3 \theta} \pm \delta_{e,h} \left[\frac{1 + 3 \sin^2 \theta}{2(ak \cos^3 \theta)^2} + \frac{2 \sin \theta}{bk^2 \cos^5 \theta} \right] \right\}, \quad (20)$$

where $\delta_e = 1$ and $\delta_h = 2$. It is seen that diffraction corrections to the field surface values in the case of *TM*-polarization (u_h) differ from the case of *TE*-polarization (u_e) by the signs \pm and by a factor of 2 in the second-order terms $\sim 1/k^2$. The spatial dependence of fields $u_{e,h}$ on coordinate $\mathbf{r} \in S$ is given by variations of surface parameters a, b and local incidence angle θ , which are functions of \mathbf{r} .

3. BACKSCATTERED FIELDS IN THE FAR ZONE

To obtain the high-frequency asymptotic expansion of backscattered fields E_{sc}, H_{sc} , we substitute the surface values of H and $\partial E/\partial n$ from (6) and (7) into (1) and (2), correspondingly, and use representation (20) for $u_{e,h}$. For the backscattering direction, in a wave zone ($kR \gg 1$) and at a long distance R essentially exceeding the curvature radius a_0 at the specular point O (for a concave surface the inequality $R \gg a_0$ guarantees that the observation point is far away from the caustics of the reflected wave field), after integration in (1) and (2) over dy in the infinite limits (implying that the body dimension in the direction of axis Oy exceeds essentially the linear size of the Fresnel zone $\sqrt{\lambda R}$ in this direction), we obtain:

$$E_{sc}, H_{sc} = \mp \sqrt{\frac{k}{8\pi i R}} e^{ikR} \int_{-\infty}^{\infty} u_{e,h}(x) e^{-2ikZ(x)} dx. \quad (21)$$

To perform integration in (21) in an explicit form, it is necessary to have $u_{e,h}$ as a function of x in a reference frame (x, y, z) related to the specular point O (Fig. 1), where the surface equation has the form $z = Z(x)$, while (20) gives $u_{e,h}$ in the local reference frame (ξ, η, ζ) . Since the reference frame (ξ, η, ζ) can be obtained from the original reference frame (x, y, z) by shifting the origin from point $O(0, 0, 0)$ to the point $O_S(x_S, 0, z_S)$ and consequent rotation by the angle θ , the following simple relations exist between coordinates (ξ, ζ) and (x, z) :

$$\begin{aligned} \xi &= (x - x_S) \cos \theta - (z - z_S) \sin \theta, \\ \zeta &= (x - x_S) \sin \theta + (z - z_S) \cos \theta. \end{aligned} \quad (22)$$

This allows us to express the local surface differential parameters a and b , introduced in (14), through the derivatives of $Z(x)$ in the original

frame of reference :

$$-\frac{1}{a} \equiv \left. \frac{d^2 z}{d\xi^2} \right|_{\xi=0} = \cos^3 \theta \left. \frac{d^2 Z}{dx^2} \right|_{x=x_S}, \quad (23)$$

$$-\frac{2}{b} \equiv \left. \frac{d^3 z}{d\xi^3} \right|_{\xi=0} = \cos^4 \theta \left. \frac{d^3 Z}{dx^3} \right|_{x=x_S} + 3 \sin \theta \cos^5 \theta \left. \left(\frac{d^2 Z}{dx^2} \right)^2 \right|_{x=x_S} \quad (24)$$

In a high-frequency limit, only the small vicinity of the specular point O is essential in integrals in (21). To obtain the expansion of scattered fields in the series of $1/k$ with accuracy $1/k^2$, i.e., to represent the scattered fields in the form:

$$E_{sc} = E^{(0)} + E^{(1)} + E^{(2)}, \quad H_{sc} = H^{(0)} + H^{(1)} + H^{(2)},$$

where $E^{(n)}, H^{(n)} \sim 1/k^n$, (25)

it is necessary to expand $Z(x)$ in series of x near the specular point O in the exponent in the integrand (21) up to the term $\sim x^6$:

$$Z(x) \simeq \sum_{n=2}^6 \frac{x^n}{n!} Z_n, \quad Z_n \equiv \left. \frac{d^n}{dx^n} Z(x) \right|_{x=0}. \quad (26)$$

In the geometrical optics limit ($k = \infty$), from (21) it follows that:

$$\left. \begin{array}{l} E^{(0)} \\ H^{(0)} \end{array} \right\} = \mp \sqrt{\frac{a_0}{2R}} e^{ikR}, \quad (27)$$

where $a_0 \equiv -\left(d^2 Z/dx^2\right)_{x=0}^{-1}$ is the surface curvature radius at the specular point O . Note that (27) is valid not only for the convex surface ($a_0 > 0$), but for the concave one also: if $a_0 < 0$, the fields (27) acquire the additional phase shift $\pi/2$ caused by the caustic.

After simple but cumbersome derivations, from (21) we obtain the following expansion of fields E and H , normalized on their geometrical optics limits $E^{(0)}$ and $H^{(0)}$, over the inverse value of a large parameter $p = a_0 k \gg 1$:

$$\left. \begin{array}{l} \bar{E} \\ \bar{H} \end{array} \right\} = 1 + \frac{i}{2p} \left(3q_4 + \frac{5!!}{2} q_3^2 \pm 1 \right) \\ \pm \frac{1}{8p^2} \left[4\delta_{e,h} + q_3^2 \left(21 \mp 9!! q_4 \mp \frac{11!!}{12} q_3^2 \right) \right. \\ \left. + q_4 (18 \mp 7!! q_4) \mp 30 (q_6 + 7q_3 q_5) \right], \quad (28)$$

where $\overline{E} = E_{sc}/E^{(0)}$, $\overline{H} = H_{sc}/H^{(0)}$ and $q_n = a_0^{n-1}Z_n/n!$. It is seen that the first-order terms $\sim 1/p$ depend not only on the surface S curvature radius a_0 at the specular point, but on surface third and fourth derivatives as well. The coefficient of the second-order term $\sim 1/p^2$ depends on the higher derivatives of $Z(x)$ up to the $d^6 Z(x)/dx^6|_{x=0}$.

3.1. Phase Corrections

The second terms in the right-hand side of (28) are the first-order corrections $\delta\phi_e$ and $\delta\phi_h$ to the phase of backscattered signals for TE and TM polarizations, correspondingly:

$$\left. \begin{matrix} \delta\phi_e \\ \delta\phi_h \end{matrix} \right\} = \frac{1}{2p} \left(3q_4 + \frac{5!!}{2} q_3^2 \pm 1 \right). \quad (29)$$

Despite the fact that these corrections depend on the third and fourth derivatives of the surface, their difference $\Delta\phi_{eh}$ depends only on the curvature radius a_0 at the specular point:

$$\Delta\phi_{eh} = \delta\phi_e - \delta\phi_h = \frac{1}{p} = \frac{1}{a_0 k}. \quad (30)$$

Note that $\Delta\phi_{eh} > 0$ for convex specular points with $a_0 > 0$, and $\Delta\phi_{eh} < 0$ for the concave ones ($a_0 < 0$). As distinct from the wave amplitude (or the scattering cross-section) the phase of the scattered field can be measured with a very high accuracy. From (30), it follows that measurement of the phase difference between TE and TM polarized scattered waves allows one to retrieve the curvature radius a_0 of the surface and its sign at the specular point.

3.2. Backscattering Cross-Sections

In 2-D geometry, when the scattered fields E, H in the far zone have the cylindrical divergence $\sim 1/\sqrt{R}$, the scattering cross-section per unit length of the surface directrix (along the axis Oy in our case) is defined by the equation (e.g., see (I.34) in [5]):

$$\sigma = \lim_{R \rightarrow \infty} 2\pi R \left| \frac{F}{F_0} \right|^2, \quad (31)$$

where $F = E_{sc}, H_{sc}$ and $F_0 = E_0, H_0$ for TE - and TM - polarized waves, correspondingly. In applications to radio wave propagation and scattering theory, the TE polarization is referred to as ‘‘horizontal’’ and is denoted as H , and TM polarization is referred to as ‘‘vertical’’

and is denoted as V . The corresponding backscattering cross-sections σ_{HH} and σ_{VV} in our notations have the form:

$$\sigma_{HH} = \lim_{R \rightarrow \infty} 2\pi R \left| \frac{E_{sc}}{E_0} \right|^2 \text{ and } \sigma_{VV} = \lim_{R \rightarrow \infty} 2\pi R \left| \frac{H_{sc}}{H_0} \right|^2. \quad (32)$$

Substituting here $E_{sc} = E^{(0)}\bar{E}$ and $H_{sc} = H^{(0)}\bar{H}$, where \bar{E} and \bar{H} are given by (28), and taking into account (27), we obtain:

$$\left. \begin{aligned} \bar{\sigma}_{HH} \\ \bar{\sigma}_{VV} \end{aligned} \right\} = 1 - \frac{1}{4p^2} [1 \mp 6 + 18q_3^2 (45q_3^2 + 50q_4 \mp 2) \\ + 24q_4 (4q_4 \mp 1) + 30 (q_6 + 7q_3q_5)], \quad (33)$$

where $\bar{\sigma}_{HH} = \sigma_{HH}/\sigma_0$, $\bar{\sigma}_{VV} = \sigma_{VV}/\sigma_0$, and $\sigma_0 = \pi|a_0|$ is the backscattering cross-section from a solitary specular point (actually, the line in 2-D case) in the geometrical optics limit $p = \infty$.

3.3. Polarization Ratio

From (33) it follows for the HH/VV ratio:

$$\frac{\sigma_{HH}}{\sigma_{VV}} \simeq 1 + \frac{3}{p^2} (1 + 6q_3^2 + 4q_4). \quad (34)$$

Note that in general, the first nonzero term $\sim 1/k^2$ in a high-frequency expansion of the polarization ratio depends not only on the curvature radius a_0 at the specular point, but on high-order ($n = 3, 4$) derivatives Z_n of the surface profile as well.

Taking into account our definitions

$$\frac{1}{a_0} = -Z_2, \quad q_3 = \frac{a_0^2}{6} Z_3, \quad q_4 = \frac{a_0^3}{24} Z_4, \quad (35)$$

from (34) we can obtain an explicit equation for the diffraction correction Δ to the polarization ratio:

$$\Delta = \frac{\sigma_{HH}}{\sigma_{VV}} - 1 = \frac{1}{2k^2} \left(6Z_2^2 + \frac{Z_3^2}{Z_2^2} - \frac{Z_4}{Z_2} \right). \quad (36)$$

It is seen that in general, Δ may be positive as well as negative, depending on the sign and the value of the term Z_4/Z_2 . As in practice, the scattering cross-sections σ_{HH} and σ_{VV} are measured in dB . The sign of the HH/VV ratio measured in dB coincides with the sign of Δ , and below we will indicate this fact, naming Δ as the HH/VV ratio or the polarization ratio itself, keeping in mind that $\frac{\sigma_{HH}}{\sigma_{VV}} (dB) \simeq 4.34\Delta$.

3.4. Dependence on the Angle of Incidence

Asymptotic expansions (28) of the backscattered fields, and all above particular equations for phase and backscattering cross-section corrections to the GO result (27), are written in a form that depends on derivatives $Z_n \equiv d^n Z(x)/dx^n$ of surface equation $Z(x)$ in the local frame of reference (x, y, z) attached to the specular point O (see Fig. 1). If we consider a plane incident wave propagating in the direction α (instead of α_0 as was previously considered), which makes an arbitrary angle θ with the axis Oz of the “laboratory” frame of reference (x, y, z) , where the surface equation has the form $z = Z(x)$, we can use all the above results with substitution of $Z_n \rightarrow z_n \equiv d^n z(\xi)/d\xi^n$, where $z(\xi)$ is the surface equation in the local frame of reference (ξ, η, ζ) , attached to the corresponding specular point O_S (see Fig. 1). To obtain the dependence of backscattered field parameters on the angle of incidence θ , it is necessary to evaluate the derivatives z_n through the derivatives Z_n at the specular point O_S , which now does not coincide with the origin O of the coordinates (x, y, z) . The transformation from the “laboratory” coordinate system (x, y, z) to the local coordinate system (ξ, η, ζ) is given by (22), which we employed above to obtain equations (23) and (24), connecting z_2 and z_3 with Z_2 and Z_3 . The full set of equations connecting z_n with Z_n for $n \leq 6$ has the form:

$$\begin{aligned}
 z_1 &= 0, \\
 z_2 &= \cos \theta Z_2 x_1^2, \\
 z_3 &= \cos \theta [Z_3 x_1^3 + 3Z_2 x_1 x_2], \\
 z_4 &= \cos \theta [Z_4 x_1^4 + 6Z_3 x_1^2 x_2 + Z_2 (3x_2^2 + 4x_1 x_3)], \\
 z_5 &= \cos \theta [Z_5 x_1^5 + 10Z_4 x_1^3 x_2 + 5Z_3 (3x_1 x_2^2 + 2x_1^2 x_3) + 5Z_2 (2x_2 x_3 + x_1 x_4)], \\
 z_6 &= \cos \theta [Z_6 x_1^6 + 15Z_5 x_1^4 x_2 + 5Z_4 (9x_1^2 x_2^2 + 4x_1^3 x_3) \\
 &\quad + 15Z_3 (x_2^3 + 4x_1 x_2 x_3 + x_1^2 x_4) + Z_2 (10x_3^2 + 15x_2 x_4 + 6x_1 x_5)]. \quad (37)
 \end{aligned}$$

Here, all derivatives Z_n are taken at the specular point $O_S(x_S, z_S)$, where $z_S = Z(x_S)$ and x_S is the solution of the equation:

$$\left. \frac{dZ(x)}{dx} \right|_{x_S} = -\tan \theta, \quad (38)$$

and derivatives $x_n \equiv d^n x/d\xi^n$ have the following explicit form:

$$\begin{aligned}
 x_1 &= \cos \theta, \\
 x_2 &= \sin \theta \cos^3 \theta Z_2, \\
 x_3 &= \sin \theta \cos^4 \theta [Z_3 + 3 \sin \theta \cos \theta Z_2^2],
 \end{aligned}$$

$$\begin{aligned}
 x_4 &= \sin \theta \cos^5 \theta \left[Z_4 + 5 \sin \theta \cos \theta Z_2 (2Z_3 + 3 \sin \theta \cos \theta Z_2^2) \right], \\
 x_5 &= \sin \theta \cos^6 \theta \left[Z_5 + 5 \sin \theta \cos \theta (3Z_4 Z_2 + 2Z_3^2) \right. \\
 &\quad \left. + 105 \sin^2 \theta \cos^2 \theta Z_2^2 (Z_3 + \sin \theta \cos \theta Z_2^2) \right].
 \end{aligned} \tag{39}$$

Substituting in (28), and in all equations that follow from it, $q_n = a^{n-1} z_n / n!$ and $p = ak$, where a is a surface curvature radius at the specular point O_S , given by the equation:

$$\frac{1}{a} = -z_2 = -\cos^3 \theta Z_2, \tag{40}$$

we obtain the high-frequency asymptotic expansion of scattered fields depending on the incidence angle θ for an arbitrary surface, which equation $Z(x)$ is given in the "laboratory" frame of reference (x, O, z) , which is not connected with the specular point O_S . In the next section, we obtain from these general equations the explicit formulae for 2-D (i.e., cylindrical) surfaces with conic section directrices.

4. ASYMPTOTIC EXPANSIONS FOR FIELDS BACKSCATTERED FROM A CYLINDER WITH A CONIC SECTION DIRECTRIX

4.1. The Circular Cylinder

We take the equation of the circular cylindrical surface in the form:

$$z^2 + x^2 = a_0^2, \quad |x| \leq a_0. \tag{41}$$

It is evident from the circular symmetry of the problem in this particular case that asymptotic expansions of backscattered fields do not depend on the incident angle θ . Therefore, it is enough to consider the case of $\theta = 0$, and take the surface equation in the form:

$$Z(x) = \sqrt{a_0^2 - x^2}, \quad |x| \leq a_0. \tag{42}$$

The specular point is located at the point $(0, a_0)$, and only the even derivatives of $Z(x)$ are not equal to zero, which results in the following formulae for q_n :

$$q_4 = -\frac{1}{8}, \quad q_6 = -\frac{1}{16}, \quad q_3 = q_5 = 0. \tag{43}$$

Substituting these equations for q_n into (28), we obtain the asymptotic expansion for backscattered fields:

$$\overline{E} = 1 + \frac{5i}{16p} + \frac{127}{512p^2}, \tag{44}$$

$$\overline{H} = 1 - \frac{11i}{16p} - \frac{353}{512p^2}. \quad (45)$$

These equations coincide with the high-frequency asymptotic expansion of exact solutions given by equations (2.31) and (2.63) in [5].

From (44) and (45), we obtain the corrections to the phases of backscattered fields:

$$\delta\phi_e = \frac{5}{16p}; \quad \delta\phi_h = -\frac{11}{16p}. \quad (46)$$

The positive phase shift $\delta\phi_e$ to the TE -polarized (horizontal polarization HH) wave is equivalent to the ray length increasing, i.e., to shifting the specular reflecting point from the actual specular point O_S *inside* the cylinder by distance $s_e = \delta\phi_e/k = 5a_0/16p^2$ to the spurious specular point O_e (see Fig. 2a). Similarly, the negative sign of $\delta\phi_h$ for the TM polarized wave (vertical polarization VV) is equivalent to shifting the reflecting point O_S *outside* the cylinder by distance $s_h = -\delta\phi_h/k = 11a_0/16p^2$, which exceeds the length of inside shifting s_e more than two times. The distance $s = s_e + s_h$ between this two spurious specular points O_e and O_h is equal to a_0/p^2 , in accordance with the general equation (30) for the phase difference $\Delta\phi_{eh}$. Note that for a concave surface in the vicinity of the specularly reflecting point O_S , the opposite situation occurs (Fig. 2b): for a TE polarized wave the spurious reflecting point shifts outside the body, and for a TM polarized wave it shifts inside.

From (33), we obtain the high-frequency expansions of the backscattering cross-sections:

$$\sigma_{HH} = \sigma_0 \left(1 + \frac{19}{32p^2} \right); \quad \sigma_{VV} = \sigma_0 \left(1 - \frac{29}{32p^2} \right), \quad (47)$$

and for the polarization ratio we have from (34):

$$\frac{\sigma_{HH}}{\sigma_{VV}} \simeq 1 + \frac{3}{2p^2}. \quad (48)$$

It is worth to note that diffraction effects result in increasing the backscattering cross-section for HH polarization and decrease it for VV polarization.

4.2. The Parabolic Cylinder

The equation for the surface of the parabolic cylinder has the form:

$$Z(x) = -\frac{x^2}{2a_0}, \quad (49)$$

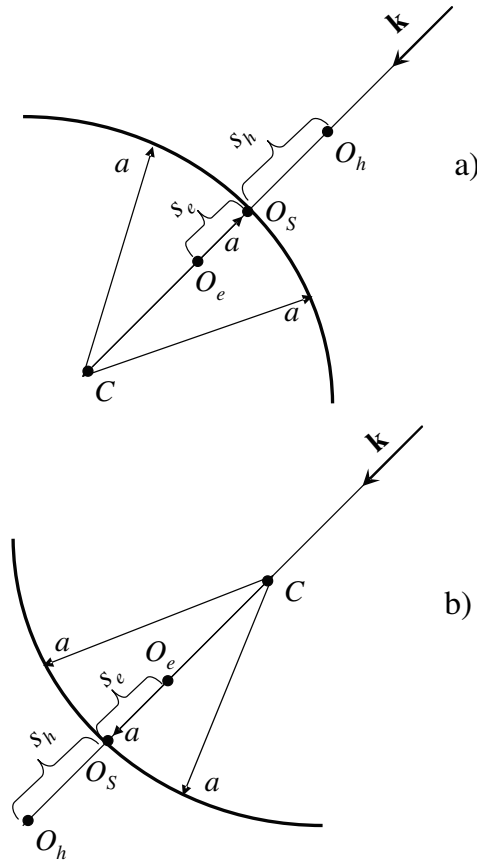


Figure 2. The interpretation of the diffraction corrections to the phases of backscattered fields as shifting of the actual specular point O_S to the spurious specular point O_e (HH polarization) and to O_h (VV polarization) for a) convex and b) concave surfaces.

where $a_0 > 0$ is the parabola curvature radius at the *apical* point O . The location of the specular point O_S is determined by the equations:

$$x_S = a_0 \tan \theta, \quad z_S = -\frac{1}{2} a_0 \tan^2 \theta. \quad (50)$$

The surface curvature radius a at the specular point O_S , determined by (40), depends on the incident angle θ :

$$a = \frac{a_0}{\cos^3 \theta}, \quad (51)$$

and the GO backscattering cross-section σ_0 increases as θ increases:

$$\sigma_0 = \pi a = \frac{\pi a_0}{\cos^3 \theta}. \quad (52)$$

All surface derivatives Z_n for $n \geq 3$ are equal to zero, and from (37) and (39) it is possible to obtain the explicit equations for z_n :

$$z_n = (-1)^{n+1} \frac{\cos^{n+1} \theta \sin^{n-2} \theta}{2^{n-2} a_0^{n-1}} (2n-3)!! \quad (53)$$

After substituting $q_n = a^{n-1} z_n / n!$, the asymptotic expansions (28) take the form:

$$\bar{E} = 1 + \frac{i}{2p} \cos^3 \theta + \frac{\cos^4 \theta (2 \cos 2\theta - \sin^2 \theta)}{4p^2}, \quad (54)$$

$$\bar{H} = 1 - \frac{i}{2p} \cos^3 \theta - \frac{\cos^4 \theta (4 \cos 2\theta + \sin^2 \theta)}{4p^2}, \quad (55)$$

where we have retained the definition $p = a_0 k$ for the large parameter introduced above. In the specific case $\theta = 0$ these equations take the simple form:

$$\bar{E} = 1 + \frac{i}{2p} + \frac{1}{2p^2}, \quad (56)$$

$$\bar{H} = 1 - \frac{i}{2p} - \frac{1}{p^2}, \quad (57)$$

which coincides with results obtained in [6] (see also Chapter 7.2 in [5]).

From (54) and (55), it follows that the corrections $\delta\phi_e$ and $\delta\phi_h$ to the GO phase of scattered fields for *TE* and *TM* waves have the same value, but differ by sign:

$$\delta\phi_e = -\delta\phi_h = \frac{\cos^3 \theta}{2p} = \frac{1}{2ak}, \quad (58)$$

and the general equation (30) for their difference holds:

$$\Delta\phi_{eh} = \delta\phi_e - \delta\phi_h = \frac{1}{ak}. \quad (59)$$

From (58) it follows that displacements s_e and s_h of the spurious specular points (see Fig. 2a), introduced in the previous subsection for a circular cylinder, are equal to each other for a parabolic cylinder:

$$s_e = s_h = \frac{a_0}{2p^2} \cos^3 \theta, \quad (60)$$

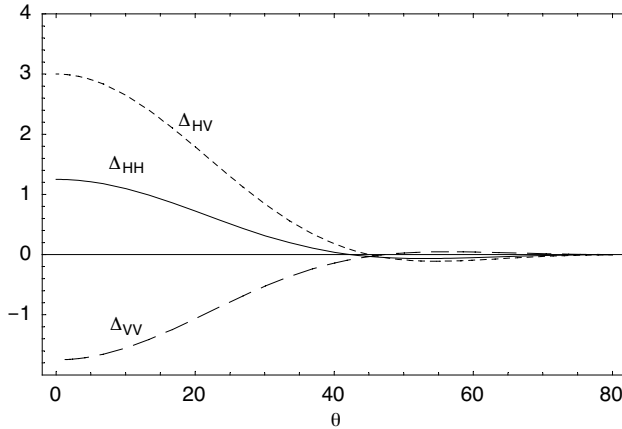


Figure 3. The dependence of diffraction corrections Δ_{HH} (solid line) and Δ_{VV} (long-dashed line) to the backscattering cross-sections from a parabolic cylinder on angle of incidence θ ; the short-dashed line corresponds to the HH/VV polarization ratio Δ_{HV} .

and the distance $s = s_e + s_h$ between them decreases rapidly as the incident angle θ increases, because of curvature radius a increasing, as it follows from (51).

The asymptotic expansions of the backscattering cross-sections, normalized on σ_0 , can be obtained directly from (54) and (55):

$$\bar{\sigma}_{HH} = 1 + \frac{\cos^4 \theta (5 \cos 2\theta - \sin^2 \theta)}{4p^2}, \quad (61)$$

$$\bar{\sigma}_{VV} = 1 - \frac{\cos^4 \theta (7 \cos 2\theta + \sin^2 \theta)}{4p^2}. \quad (62)$$

The dependence on the angle of incidence θ of the diffraction corrections $\Delta_{HH} = p^2 (\bar{\sigma}_{HH} - 1)$ and $\Delta_{VV} = p^2 (\bar{\sigma}_{VV} - 1)$ to the GO backscattering cross-sections, normalized by the factor p^2 , is depicted in Fig. 3. It is seen that, as the incident angle θ increases, the diffraction corrections for the backscattering cross-sections decrease rapidly (as $\sim \cos^6 \theta$) from their absolute maximum values $\Delta_{HH} = 5/4$ and $\Delta_{HH} = -7/4$ at $\theta = 0$. With the further increasing of θ , they change the sign at $\theta_{pH} = \arctan(\sqrt{5/6}) \simeq 42.4^\circ$ for $\bar{\sigma}_{HH}$, and at $\theta_{pV} = \arctan(\sqrt{7/6}) \simeq 47.2^\circ$ for $\bar{\sigma}_{VV}$, and then they tend to zero when $\theta \rightarrow \pi/2$.

For the polarization ratio, from (61) and (62) it follows:

$$\frac{\sigma_{HH}}{\sigma_{VV}} \simeq 1 + \frac{3 \cos^4 \theta \cos 2\theta}{p^2}. \quad (63)$$

The normalized correction to the polarization ratio $\Delta_{HV} = p^2 \Delta$, where Δ is introduced in (36) as $\Delta = \sigma_{HH}/\sigma_{VV} - 1$, is shown in Fig. 3 by the short-dashed line. It also decreases as $\sim \cos^6 \theta$ from its maximal value $\Delta_{HV} = 3$ at $\theta = 0$, and changes sign at $\theta = 45^\circ$. The similar rapid decrease of the polarization ratio ($\sim \cos^6 \theta$) was obtained in [18] for backscattering from a statistically rough surface after statistical averaging.

It is easy to obtain all the above parameters averaged over the incident angle θ (or parabola axis Oz orientation relative to the direction of incident wave propagation) in the interval $(-\pi/2, \pi/2)$:

$$\langle \delta\phi_e \rangle = -\langle \delta\phi_h \rangle = \frac{1}{2p} \langle \cos^3 \theta \rangle = \frac{2}{3\pi p}, \quad \langle \Delta\phi_{eh} \rangle = \frac{4}{3\pi p}, \quad (64)$$

$$\langle \Delta_{HH} \rangle = \frac{19}{64}, \quad \langle \Delta_{VV} \rangle = -\frac{29}{64}, \quad \langle \Delta_{HV} \rangle = \frac{3}{4}, \quad (65)$$

where $\langle \dots \rangle$ denotes the angular averaging:

$$\langle f(\theta) \rangle = \frac{1}{\pi} \int_{-\pi/2}^{\pi/2} f(\theta) d\theta. \quad (66)$$

Note that the averaged diffraction corrections (65) to the backscattering cross-sections from the parabolic cylinder with curvature radius a_0 at the apical point O , are exactly two times smaller in comparison with those (47), (48) for a circular cylinder with the same radius.

It is worth emphasizing that diffraction corrections Δ_{HH} , Δ_{VV} to the backscattering cross-sections are normalized by the GO backscattering cross-section $\sigma_0(\theta)$ (52), which tends to infinity as $(\pi/2 - \theta)^{-3}$ when $\theta \rightarrow \pi/2$, and $\langle \sigma_0(\theta) \rangle = \infty$ because of divergency of the integral (66). This divergency is caused by increasing the local curvature radius a at the specular point O_S as $a_0/\cos^3 \theta$ when $\theta \rightarrow \pi/2$. All our consideration is based on the assumption that $R \gg a$, which restricts the applicability of the results obtained above by the incident angles θ far enough from $\pi/2$: $\cos \theta \gg (a_0/R)^{1/3}$.

4.3. The Elliptic Cylinder

We choose the ellipse equation in the form:

$$\frac{z^2}{c^2} + \frac{x^2}{b^2} = 1, \quad c \geq b. \quad (67)$$

Here, b is the length of a small semi-axis, c is the length of a large semi-axis (usually it is denoted as a , but we retain this notation for the local curvature radius at the specularly reflecting point O_S). Because of the ellipse symmetry relative to the axes Oz and Ox , we can consider the incident angles θ only in the interval $(0, \pi/2)$, and take the surface equation $Z(x)$ in the form:

$$Z(x) = \sqrt{c^2 - \frac{x^2}{r^2}}, \quad r = \frac{b}{c} \leq 1, \quad |x| \leq b. \quad (68)$$

The semi-axis ratio r is connected with the ellipse eccentricity ϵ by the relation $r = \sqrt{1 - \epsilon^2}$, so that $r = 1$ corresponds to the circle, and $r = 0$ corresponds to the parabola with the axis of symmetry Oz . It is convenient, for simplification of the equation below, to introduce the curvature radius a_0 at the apical (top) point $O(0, c)$ of the surface:

$$a_0 = \frac{b^2}{c} = br = cr^2, \quad (69)$$

and rewrite (68) in the form:

$$Z(x) = \frac{1}{r} \sqrt{a_0^2 - r^2 x^2}. \quad (70)$$

The location of the specular reflecting point $O_S(x_S, z_S)$ at the surface is determined by equation (38), the solution of which has the form:

$$x_S = \frac{a_0 \tan \theta}{\sqrt{1 + r^2 \tan^2 \theta}}, \quad z_S = Z(x_S), \quad (71)$$

and for the derivatives $Z_n \equiv d^n Z / dx^n$ of the surface equation (70) at the specular reflecting point O_S , we obtain:

$$\begin{aligned} Z_2 &= -\frac{(1 + r^2 \tan^2 \theta)^{3/2}}{a_0}, \\ Z_3 &= -3 \frac{r^2}{a_0^2} \tan \theta (1 + r^2 \tan^2 \theta)^2, \\ Z_4 &= -3 \frac{r^2}{a_0^3} (1 + 5r^2 \tan^2 \theta) (1 + r^2 \tan^2 \theta)^{5/2}, \\ Z_5 &= -15 \frac{r^4}{a_0^4} \tan \theta (3 + 7r^2 \tan^2 \theta) (1 + r^2 \tan^2 \theta)^3, \\ Z_6 &= -45 \frac{r^4}{a_0^5} (1 + 14r^2 \tan^2 \theta + 21r^4 \tan^4 \theta) (1 + r^2 \tan^2 \theta)^{7/2}. \end{aligned} \quad (72)$$

The curvature radius a at the specular reflecting point O_S is determined by (40):

$$a(\theta) = \frac{a_0}{(\cos^2 \theta + r^2 \sin^2 \theta)^{3/2}}, \quad (73)$$

and in the GO optics limit the backscattering cross-section (for both polarizations) takes the form:

$$\sigma_0(\theta) = \frac{\pi a_0}{(\cos^2 \theta + r^2 \sin^2 \theta)^{3/2}}. \quad (74)$$

For $r = 1$, (74) coincides with the backscattering cross-section $\sigma_0 = \pi a_0$ from the circular cylinder, and for $r = 0$ it transforms into (52) for the parabolic cylinder. For an arbitrary value of r in the interval $[0, 1]$ and $\theta = 0$, the backscattering cross-section (74) is equal to the one for the circular cylinder with radius a_0 , and for $\theta = \pi/2$ it transforms into the backscattering cross-section from the circular cylinder with radius $a(\pi/2) = a_0/r^3 = c^2/b$.

Averaging (74) over all the possible angles of incidence θ (or over the arbitrary orientations of ellipse relative to the direction of the incident wave), according to definition (66), leads to the formula:

$$\langle \sigma_0(\theta) \rangle = \frac{L}{2}, \quad (75)$$

where $L = 4cE(\epsilon^2)$ is the ellipse circumference, and $E(\epsilon^2)$ is a complete elliptic integral of the second kind (e.g., [22], Chapter 17.4):

$$E(\epsilon^2) = \int_0^{\pi/2} (1 - \epsilon^2 \sin^2 \theta)^{1/2} d\theta. \quad (76)$$

It is easy to prove that equation (75) is valid not only for an elliptic cylinder, but for a cylinder with an arbitrary convex directrix having length L . For a 3-D case, the analogous general result was recently obtained by A. G. Voronovich (private communication): the scattering cross-section from an arbitrary convex body in a GO limit (disregarding absorption and multiple reflections inside the body), averaged over its orientation, is equal to $|V|^2 S/4$, where S is the area of the body surface and V is the Fresnel reflection coefficient at appropriate polarization.

Substituting the set of Z_n given by (72) into (39) and (37), we obtain the explicit equations for the surface profile derivatives z_n at the local frame of reference at the specularly reflecting point O_S . To obtain the high-frequency expansions of the backscattered field, we can

employ the general equation (28), where we set $q_n = a^{n-1}z_n/n!$ and substitute p by ak .

The first order $\sim 1/k$ terms in (28) give the following equations for the diffraction corrections $\delta\phi_e$ and $\delta\phi_h$ to the GO phase of the scattered fields and for their difference $\Delta\phi_{eh}$:

$$\delta\phi_e = \frac{8(\cos^2\theta + r^2\sin^2\theta)^2 - 3r^2}{16p(\cos^2\theta + r^2\sin^2\theta)^{1/2}}, \quad (77)$$

$$\delta\phi_h = -\frac{8(\cos^2\theta + r^2\sin^2\theta)^2 + 3r^2}{16p(\cos^2\theta + r^2\sin^2\theta)^{1/2}}, \quad (78)$$

$$\Delta\phi_{eh} = \delta\phi_e - \delta\phi_h = \frac{(\cos^2\theta + r^2\sin^2\theta)^{3/2}}{p} = \frac{1}{ak}, \quad (79)$$

where $p = a_0k$, as it is everywhere above. It is easy to verify that in the limiting cases $r = 1$ and $r = 0$ these equations transform to (46), (58) and (59) obtained above for circular and parabolic cylinders, correspondingly. Averaging these equations over all the incident angles θ gives the following results:

$$\langle\delta\phi_e\rangle = \frac{1}{24\pi p} [16(1+r^2)E(\epsilon^2) - 17r^2K(\epsilon^2)], \quad (80)$$

$$\langle\delta\phi_h\rangle = -\frac{1}{24\pi p} [16(1+r^2)E(\epsilon^2) + r^2K(\epsilon^2)], \quad (81)$$

$$\langle\Delta\phi_{eh}\rangle = \frac{2}{3\pi p} [2(1+r^2)E(\epsilon^2) - r^2K(\epsilon^2)], \quad (82)$$

where $K(\epsilon)$ is a complete elliptic integral of the first kind:

$$K(\epsilon^2) = \int_0^{\pi/2} (1 - \epsilon^2\sin^2\theta)^{-1/2} d\theta. \quad (83)$$

The dependence of the averaged phase corrections (80), (81) and (82) on the semi-axis ratio is depicted in Fig. 4.

From the general equation (33), we obtain the expansions of the backscattering cross-sections and HH/VV polarization ratio normalized by their GO limit (74):

$$\left. \begin{array}{l} \bar{\sigma}_{HH} \\ \bar{\sigma}_{VV} \end{array} \right\} = 1 + \frac{1}{512p^2(\cos^2\theta + r^2\sin^2\theta)} \sum_{n=0}^4 \left\{ \begin{array}{l} A_{2n}^H \\ A_{2n}^V \end{array} \right\} \cos(2n\theta), \quad (84)$$

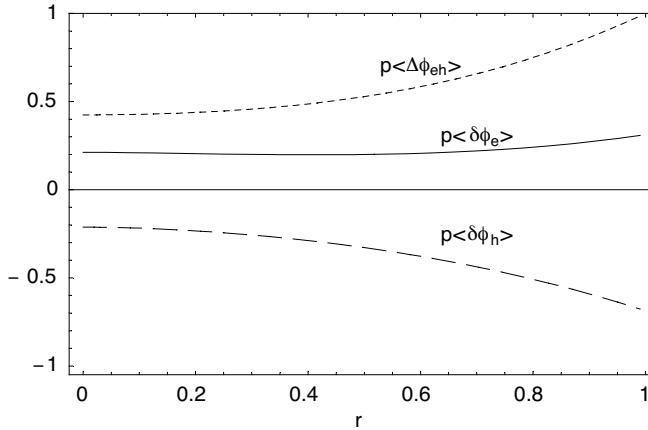


Figure 4. The phase corrections for backscattered fields from the elliptic cylinder, averaged over all incident angles θ , as functions of the ellipse semi-axis ratio r : for HH polarization (solid line), for VV polarization (long-dashed line), and for the phase difference between them (short-dashed line). The left-hand side of these plots corresponds to the parabolic cylinder ($r = 0$) and the right-hand side corresponds to the circular cylinder ($r = 1$).

where coefficients A_{2n}^H and A_{2n}^V have the form:

$$\begin{aligned}
 A_0^H &= 145(1 + r^8) - 20r^2(1 + r^4) + 54r^4, \\
 A_2^H &= -64[4(1 - r^8) - r^2(1 - r^4)], \\
 A_4^H &= 4(1 - r^2)^2[41(1 + r^4) + 50r^2], \\
 A_6^H &= 64(1 - r^4)(1 - r^2)^2, \quad A_8^H = 11(1 - r^2)^4, \quad (85)
 \end{aligned}$$

$$\begin{aligned}
 A_0^V &= -215(1 + r^8) - 20r^2(1 + r^4) + 6r^4, \\
 A_2^V &= -16[23(1 - r^8) - 2r^2(1 - r^4)], \\
 A_4^V &= -20(1 - r^2)^2[11(1 + r^4) + 14r^2], \\
 A_6^V &= -80(1 - r^2)^3(1 + r^2), \quad A_8^V = -13(1 - r^2)^4. \quad (86)
 \end{aligned}$$

For $\theta = 0$, from these equations it follows:

$$\bar{\sigma}_{HH} = 1 + \frac{1}{4p^2} \left(5 - 3r^2 + \frac{3}{8}r^4 \right), \quad (87)$$

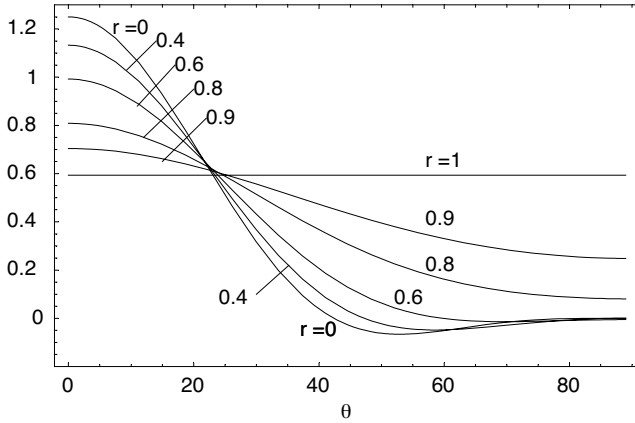


Figure 5. The dependence of diffraction corrections Δ_{HH} (horizontal polarization) to the backscattering cross-sections from the elliptical cylinder on the angle of incidence θ for different semi-axis ratio r .

$$\bar{\sigma}_{VV} = 1 - \frac{1}{4p^2} \left(7 - 3r^2 - \frac{3}{8}r^4 \right). \quad (88)$$

The expansions for $\theta = \pi/2$ can be obtained from (87) and (88) directly, only by changing the notations for semi-axes $c \Leftrightarrow b$, i.e., by replacing $r \rightarrow 1/r$, $a_0 \rightarrow c^2/b = a_0/r^3$ and $p \rightarrow p/r^3$:

$$\bar{\sigma}_{HH} = 1 + \frac{r^2}{4p^2} \left(5r^4 - 3r^2 + \frac{3}{8} \right), \quad (89)$$

$$\bar{\sigma}_{VV} = 1 - \frac{r^2}{4p^2} \left(7r^4 - 3r^2 - \frac{3}{8} \right). \quad (90)$$

The dependence of diffraction corrections $\Delta_{HH} = p^2(\bar{\sigma}_{HH} - 1)$ and $\Delta_{VV} = p^2(\bar{\sigma}_{VV} - 1)$ on the incidence angle θ is depicted in Fig. 5 (HH polarization) and Fig. 6 (VV polarization) for the set of parameter r . The horizontal lines for $r = 1$ correspond to the circular cylinder values $19/32 \simeq 0.59$ and $-29/32 \simeq -0.91$ for Δ_{HH} and Δ_{VV} , according to (47). The curves for $r = 0$ correspond to the parabolic cylinder and they coincide with the solid and long-dashed lines depicted in Fig. 3 for HH and VV polarizations, correspondingly. It is worth emphasizing that all curves in Fig. 5 and Fig. 6 correspond to ellipses with a different semi-axis ratio r , but with the same curvature radius a_0 at the apical point $O(0, c)$, which is the specularly reflecting point for $\theta = 0$. Despite the fact that all ellipses have the same curvature at the specular point O , the diffraction corrections Δ_{HH} and Δ_{VV} to the backscattering

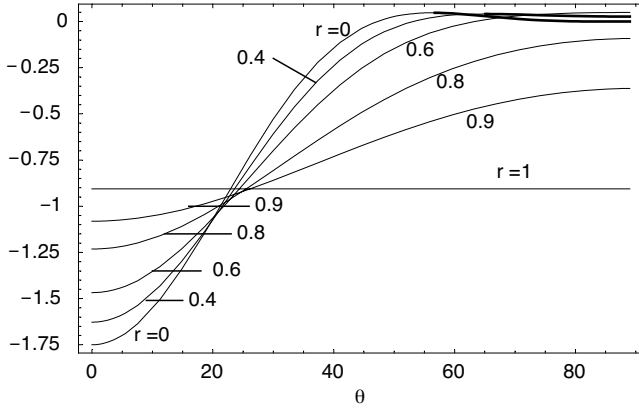


Figure 6. The same as in Fig. 5, except for Δ_{VV} (vertical polarization).

cross-sections at $\theta = 0$ are different, because of the difference of the high-order derivatives of the surface profile: they are maximal for the parabola ($r = 0$) and minimal for the circle ($r = 1$). The diffraction corrections Δ_{HH} and Δ_{VV} for the circle with radius a_0 and for the parabola, with the same curvature radius a_0 at the top, are equal to each other at incident angles $\theta_H \simeq 23.0536^\circ$ and $\theta_V \simeq 22.892^\circ$, correspondingly, which are the solutions of the cubic equations for $\cos^2 \theta$:

$$11 \cos^6 \theta_H - 6 \cos^4 \theta_H = \frac{19}{8}, \tag{91}$$

$$13 \cos^6 \theta_V - 6 \cos^4 \theta_V = \frac{29}{8}, \tag{92}$$

which are obtained by comparing the diffraction corrections (61), (62) for the parabolic cylinder with those (47) for the circular cylinder. From Fig. 5 and Fig. 6 it is seen that diffraction corrections Δ_{HH} and Δ_{VV} for ellipses with arbitrary semi-axis ratio r in the whole interval ($1 \geq r \geq 0$) almost coincide in the small vicinity of angles θ_H and θ_V , i.e., they do not depend on r and are equal to the corresponding values $19/32 \simeq 0.59$ and $-29/32 \simeq -0.91$ for a circular cylinder with a curvature radius a_0 , which is equal to the ellipse curvature radius at the top.

For the polarization ratio, it follows from (36):

$$\frac{\sigma_{HH}}{\sigma_{VV}} \simeq 1 + \frac{3 (\cos^2 \theta + r^2 \sin^2 \theta)}{4p^2}$$

$$\cdot \left[1 + r^4 + 2(1 - r^4) \cos 2\theta + (1 - r^2)^2 \cos 4\theta \right]. \quad (93)$$

The dependence of the diffraction corrections $\Delta_{HV} = p^2 (\sigma_{HH}/\sigma_{VV} - 1)$ on the polarization ratio on the angle of incidence θ is depicted in Fig. 7. For $\theta = 0$, it follows from (93):

$$\Delta_{HV} = 3 \left(1 - \frac{r^2}{2} \right). \quad (94)$$

In two limiting cases $r = 0$ and $r = 1$, this equation gives the polarization ratio $\Delta_{HV} = 3$ and $\Delta_{HV} = 1.5$ for the parabolic and circular cylinders correspondingly.

The diffraction correction Δ_{HV} for a circle ($r = 1$) with radius a_0 and for a parabola ($r = 0$), with the same curvature radius a_0 at the top, are equal to each other at the incident angle $\theta_{HV} \simeq 22.9616^\circ$, which is the solution of the cubic equation for $\cos^2 \theta$:

$$4 \cos^6 \theta_{HV} - 2 \cos^4 \theta_{HV} = 1. \quad (95)$$

This equation follows from comparison of (63) with (48), which give the polarization ratio for a parabolic and a circular cylinder, correspondingly. It is seen from Fig. 7, that for all ellipses with the semi-axis ratio r in the interval $(0, 1)$ (i.e., from the parabolic to the circular cylinder), in the vicinity of the incidence angle $\theta \simeq \theta_H \simeq \theta_V \simeq \theta_{HV} \simeq 23^\circ$, the polarization ratio Δ_{HV} takes the same value $3/2$, as for the circular cylinder with radius a_0 (48).

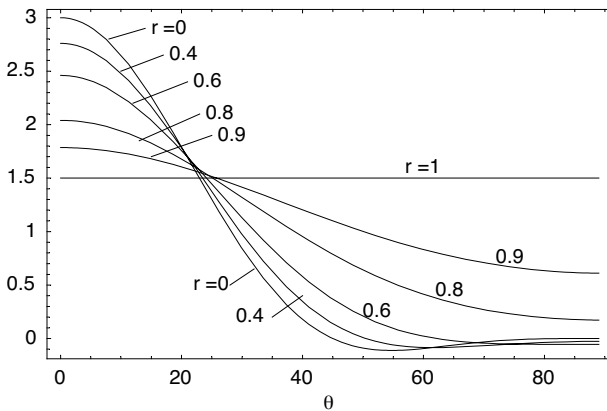


Figure 7. The same as in Fig. 5, except for HH/VV polarization ratio Δ_{HV} .

Polarization ratio Δ_{HV} , being positive at $\theta = 0$ (see (94)), decreases as the incident angle θ increases. It can vanish and change the sign at some angle of incidence θ_0 , where the expression into the square brackets in (93) turns to zero. The corresponding equation for θ_0 has the solution:

$$\cos 2\theta_0 = -\frac{r^2}{1-r^2}. \quad (96)$$

It is seen that Δ_{HV} can change the sign only for ellipses with semi-axis ratio r limited by an inequality $r \leq 1/\sqrt{2}$. When r increases from $r = 0$ (parabola) to $r = 1/\sqrt{2}$, the incident angle θ_0 , where $\Delta_{HV} = 0$, changes from $\pi/4$ (for the parabola) to $\pi/2$ (for an ellipse with the semi-axis ratio $r = 1/\sqrt{2}$). For ellipses with $1 \geq r \geq 1/\sqrt{2}$, the polarization ratio is always positive.

Direct averaging of Δ_{HH} , Δ_{VV} and Δ_{HV} over all possible incidence angles θ in the interval $(0, \pi/2)$, or over all possible ellipse orientations, leads to the following simple results:

$$\langle \Delta_{HH} \rangle = \frac{1}{64} \left[19(1+r^6) - 3r^2(1-r)^2 \right], \quad (97)$$

$$\langle \Delta_{VV} \rangle = -\frac{1}{64} \left[29(1+r^6) + 3r^2(1-r)^2 \right], \quad (98)$$

$$\langle \Delta_{HV} \rangle = \frac{3}{4} (1+r^6). \quad (99)$$

It is easy to ascertain that in the limiting cases $r = 0$ and $r = 1$, these equations give the values obtained above for parabolic (65) and circular cylinders (47), (48), correspondingly. The dependence of the averaged diffraction corrections (97)–(99) on the incidence angle is depicted in Fig. 8. It is worth noting that all of them depend very slowly on the semi-axis ratio r in the wide range of r : from $r = 0$ (parabola) to $r \simeq 0.8$ (ellipse with an eccentricity of $\epsilon \simeq 0.6$).

4.4. The Hyperbolic Cylinder

As distinct from the previous cases, there is no exact solution for plane incident wave diffraction by a hyperbolic cylinder. The only known exact result is for the field produced by a line source parallel to the axis Oy (e.g., Chapter 5 in [5]). The directrix equation for the convex hyperbolic cylinder has the form:

$$\frac{z^2}{c^2} - \frac{x^2}{b^2} = 1, \quad (100)$$

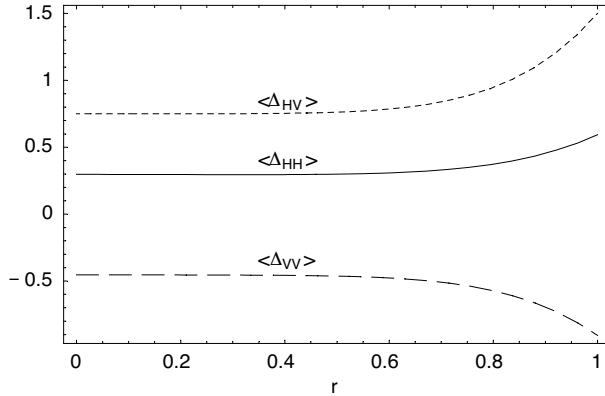


Figure 8. The diffraction corrections to the backscattering cross-sections from the elliptic cylinder, averaged over all incident angles θ , as functions of the ellipse semi-axis ratio r : $\langle \Delta_{HH} \rangle$ for HH polarization (solid line), $\langle \Delta_{HV} \rangle$ for VV polarization (long-dashed line), and $\langle \Delta_{VV} \rangle$ for the HH/VV polarization ratio (short-dashed line).

and we choose only one branch of its solution:

$$Z(x) = -\sqrt{c^2 + \frac{x^2}{r^2}}, \quad r \equiv \frac{b}{c} \geq 0, \quad -\infty < x < \infty, \quad (101)$$

which has two linear asymptotes when $x \rightarrow \pm\infty$:

$$Z(x) = -\frac{|x|}{r}, \quad |x| \rightarrow \infty. \quad (102)$$

As distinct from the ellipse equation (68), the parameter r is connected with the hyperbola eccentricity ϵ by the formula $\epsilon = \sqrt{1 + r^2}$, and it does not have the meaning of the semi-axis ratio in this subsection. The corner angle ψ between asymptotes (102) can be expressed through the parameter r by the relation:

$$\psi = \pi - 2 \arctan \left(\frac{1}{r} \right), \quad (103)$$

from which it is seen that parameter r characterize the “sharpness” of the hyperbola: when $r \rightarrow 0$, then the angle ψ between asymptotes (102) tends to $\psi \rightarrow 0$, and the hyperbola transforms into parabola (which can be considered as a sharpest hyperbola); in the opposite

limiting case $r \rightarrow \infty$, the asymptotes (102) make a very obtuse corner angle ($\psi \rightarrow \pi$), i.e., the hyperbola transforms into the plane $z = -c$. Here, we consider the assemblage of parabolas with a constant curvature radius $a_0 = b^2/c$ at the apical point $x = 0$, and with varying parameter r .

Note that (101) differs from the ellipse equation (68) only by the sign before the factor r^2 . Therefore, all analytical results obtained in the previous subsection for the elliptic cylinder can be applied for the hyperbolic cylinder only by a formal substitution $r^2 \rightarrow -r^2$ in the equations obtained above for an elliptic cylinder. In particular, the position of the specularly reflecting point O_S at the hyperbolic cylinder, illuminated by the plane wave at the incident angle θ (see Fig. 1), is given by the equation:

$$x_S = \frac{a_0 \tan \theta}{\sqrt{1 - r^2 \tan^2 \theta}}, \quad z_S = Z(x_S), \quad (104)$$

which is similar to (71). The only significant difference between the elliptic and hyperbolic cylinders is that at the surface of the elliptic cylinder the specularly reflecting point O_S in the backscattering direction exists for every incident angle θ , and its position is given by (71), whereas for the hyperbolic cylinder, it exists only for incident angles θ limited by the condition $r \tan \theta < 1$, which follows from (104). When $\theta \rightarrow \theta_m = \arctan(1/r)$, the local curvature radius a at the specularly reflecting point O_S tends to infinity (as follows from (73), where $r^2 \rightarrow -r^2$):

$$a(\theta) = \frac{a_0}{(\cos^2 \theta - r^2 \sin^2 \theta)^{3/2}}, \quad (105)$$

and the GO backscattering cross-section $\sigma_0(\theta) = \pi a(\theta)$, as well as diffraction corrections to it, tends to infinity also.

The first-order ($\sim 1/p$, where $p = a_0 k$) terms in a general equation (28) correspond to the diffraction corrections $\delta\phi_e$ and $\delta\phi_h$ to the phases of backscattered fields at two polarizations, which are given by (77) and (78) with the replacement $r^2 \rightarrow -r^2$. The phase difference $\Delta\phi_{eh}$ between HH and VV backscattered fields is equal to $1/(ak)$, where the local curvature radius a at the backscattering specular point O_S is given by (105).

The diffraction corrections to the backscattering cross-sections are given by (84)–(88) with substitution $r^2 \rightarrow -r^2$. In particular, at $\theta = 0$ we have from (87) and (88):

$$\bar{\sigma}_{HH} = 1 + \frac{1}{4p^2} \left(5 + 3r^2 + \frac{3}{8}r^4 \right), \quad (106)$$

$$\bar{\sigma}_{VV} = 1 - \frac{1}{4p^2} \left(7 + 3r^2 - \frac{3}{8}r^4 \right). \quad (107)$$

For $r = 0$, these equations coincide with (61) and (62) for a parabolic cylinder. Note that in (106) and (107), parameter r is not limited by the inequality $r \leq 1$, as was the case in the previous subsection for the elliptic cylinder, and it can be arbitrarily large for a hyperbola with a very obtuse corner angle ψ (103) between its asymptotes. The case $r = 1$ now corresponds not to the circular cylinder, as was the case in the previous sections, but to a hyperbola with orthogonal asymptotes, i.e., to a wedge with corner angle $\psi = \pi/2$ and the curvature radius a_0 at the apical point.

From (106) it follows that the diffraction correction for $\bar{\sigma}_{HH}$ is always positive at $\theta = 0$ and it increases $\sim r^4$ for $r \gg 1$, i.e., for hyperbolas with a very obtuse corner angle ($\psi \rightarrow \pi$). It is caused by the fact that the higher ($n > 2$) derivatives Z_n of the hyperbola, with a constant curvature radius a_0 at the top, increase very fast $\sim r^{n-2}$ as parameter r increases, as follows from (72) for $\theta = 0$ after replacement $r^2 \rightarrow -r^2$:

$$Z_2 = -\frac{1}{a_0}, \quad Z_4 = -3\frac{r^2}{a_0^3}, \quad Z_6 = -45\frac{r^4}{a_0^5}, \quad Z_{2n+1} = 0, \quad n = 1, 2, 3, \dots \quad (108)$$

The diffraction correction for $\bar{\sigma}_{VV}$ is negative for small r , and it changes the sign at $r \simeq 3.1445$, which is a solution of the equation

$$7 + 3r^2 - \frac{3}{8}r^4 = 0, \quad (109)$$

and $\bar{\sigma}_{VV}$, like $\bar{\sigma}_{HH}$, increases $\sim r^4$ for $r \gg 1$ with the same coefficient $3/(32p^2)$ as the diffraction correction for $\bar{\sigma}_{HH}$. In Fig. 9 and Fig. 10, the normalized diffraction corrections $\Delta_{HH} = p^2(\bar{\sigma}_{HH} - 1)$ and $\Delta_{VV} = p^2(\bar{\sigma}_{VV} - 1)$ are depicted as functions of the incidence angle θ for the set of parameter r . It is seen that, similar to the graphs depicted in Fig. 5 and Fig. 6 for an elliptic cylinder, the diffraction corrections in the case of a hyperbolic cylinder are not sensitive to the value of parameter r in the vicinity of some specific angle of incidence $\theta \simeq 20^\circ$. All corrections unrestrictedly increase as $1/(\theta - \theta_m)$ when incidence angle θ approaches the critical angle $\theta_m = \arctan(1/r)$.

For the polarization ratio, it follows from (93) after replacing $r^2 \rightarrow -r^2$:

$$\frac{\sigma_{HH}}{\sigma_{VV}} \simeq 1 + \frac{3(\cos^2 \theta - r^2 \sin^2 \theta)}{4p^2} \cdot \left[1 + r^4 + 2(1 - r^4) \cos 2\theta + (1 + r^2)^2 \cos 4\theta \right]. \quad (110)$$

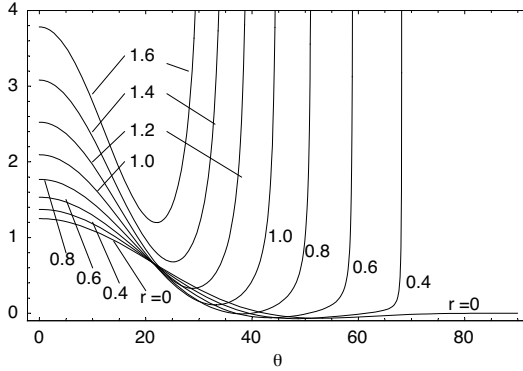


Figure 9. The dependence of diffraction corrections Δ_{HH} (horizontal polarization) to the backscattering cross-sections from the hyperbolic cylinder on the angle of incidence θ for different hyperbola parameters r .

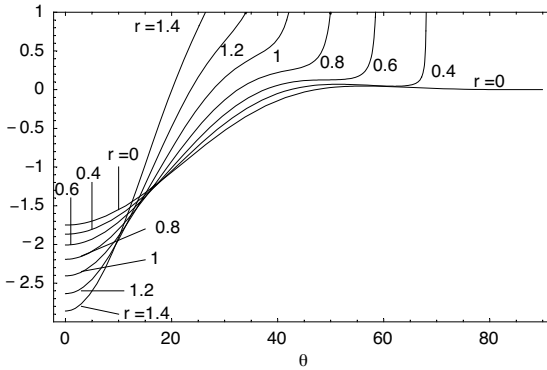


Figure 10. The same as in Fig. 9, except for Δ_{VV} (vertical polarization).

The dependence of the diffraction correction $\Delta_{HV} = p^2 (\sigma_{HH}/\sigma_{VV} - 1)$ on the angle of incidence θ for the set of parameter r into the interval $(1.4 \geq r \geq 0)$ is depicted in the upper panel of Fig. 11. It is seen that the value of Δ_{HV} is not sensitive to the parameter r in the vicinity of some incident angle θ_{HV} which can be determined as an intersection of two curves corresponding to $r = 0$ (parabola) and to $r = 1$ (hyperbola with orthogonal asymptotes $\psi = \pi/2$). The equation for this angle has the form:

$$7 \cos^2 2\theta - 2 \cos 2\theta - 3 = 0, \tag{111}$$

and for its solution we obtain $\theta_{HV} \simeq 17.81^\circ$.

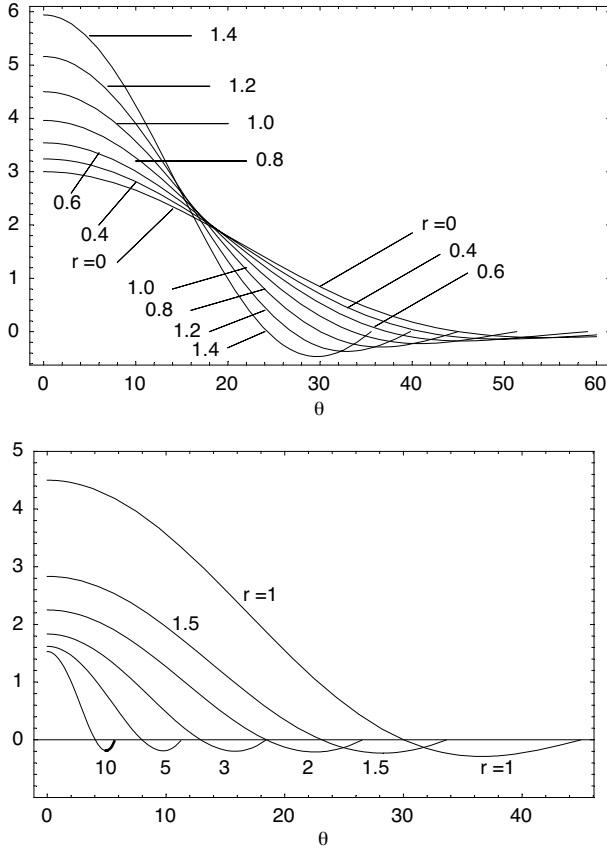


Figure 11. The same as in Fig. 9, except for the HH/VV polarization ratio Δ_{HV} . Lines in the lower panel correspond to normalized polarization ratio Δ_{HV}/r^2 .

For $\theta = 0$, it follows from (110):

$$\Delta_{HV} = 3 \left(1 + \frac{r^2}{2} \right), \quad (112)$$

which also can be obtained from (94) by replacing $r^2 \rightarrow -r^2$. For $r^2 \gg 1$ the diffraction correction (112) increases $\sim r^2$, as distinct from the corrections to the backscattering cross-sections (106) and (107) which increase as $\sim r^4$. At $\theta = 0$ the polarization ratio is always positive, and it decreases as incident angle θ increases. It vanishes and then changes the sign at the incident angle θ_0 , given by the equation,

similar to (96):

$$\cos 2\theta_0 = \frac{r^2}{1+r^2}, \quad (113)$$

which has a solution θ_0 for all possible values of parameter r . This angle of incidence θ_0 decreases monotonically as parameter r increases from $\theta_0 = \pi/4$ for $r = 0$ (parabolic cylinder) to $\theta_0 = \pi/6$ for $r = 1$ (hyperbola with orthogonal asymptotes $\psi = \pi/2$) and tends to zero for $r \rightarrow \infty$. The dependence of the diffraction correction $\Delta_{HV} = p^2 (\sigma_{HH}/\sigma_{VV} - 1)$, normalized by the factor r^2 , on the angle of incidence θ for the set of parameter r into the interval ($10 \geq r \geq 1$) is depicted in the lower panel of Fig. 11. Note that the normalized by r^2 polarization ratio Δ_{HV}/r^2 at $\theta = 0$ monotonically decreases from 4.5 for $r = 1$ to 1.5 for $r \rightarrow \infty$. In contrast to corrections to the backscattering cross-sections Δ_{HH} and Δ_{VV} , which tend to infinity as $1/(\theta - \theta_m)$ when incidence angle θ approaches the critical angle $\theta_m = \arctan(1/r)$, the polarization ratio Δ_{HV} tends to zero when $\theta \rightarrow \theta_m$, being negative in the interval $\theta_m \geq \theta \geq \theta_0$.

5. CONCLUSIONS

With consecutive iterations of the exact integral equations, we obtained the high-frequency asymptotic expansions of the tangent component of a magnetic field and the normal derivative of an electric field at a perfectly conducting smooth surface illuminated by a plane incident wave. The first-order corrections $\sim 1/k$ to their GO values (which are equal to doubled corresponding values in the incident field) are determined only by the surface local curvature radius a and the local incident angle θ , and they differ only by sign for *TE*- and *TM*- polarized waves. The second-order corrections $\sim 1/k^2$ depend also on the local third derivative of the surface, and for *TE*- and *TM*- polarized waves they differ not only by sign but also by a factor of 2 (doubled for *TM*-polarized wave).

The scattered fields in the far zone were obtained, according to the Huygens-Kirchhoff principle, by integrating over the surface the corresponding surface values of a magnetic field and the normal derivative of an electric field. As a result of these derivations, we have found that the first-order corrections $\sim 1/k$ to the GO values of the backscattered fields (which are fully determined by the surface curvature radius a_0 at the specularly reflecting point) depend on the 3rd and 4th surface derivatives, whereas the second-order corrections $\sim 1/k^2$ depend also on the 5th and 6th surface derivatives.

The first-order terms $\sim 1/k$ in these asymptotic expansions are orthogonal to their GO values and they give the diffraction corrections

to the phase of backscattered fields. The phase difference between TE and TM polarized waves is determined only by the surface curvature radius a at the specularly reflecting point, and it is equal to the inverse value of a large parameter $p = ak$.

The first nonzero correction term to the backscattering cross-sections has the order of $\sim 1/k^2$, and it depends on all derivatives of the surface at the specular reflecting point up to the 6th order. In the HH/VV polarization ratio, some of these terms are cancelled out, and the HH/VV ratio depends only on the 2nd, 3rd and 4th local derivatives of the surface.

We applied these general results to the specific case of backscattering by a cylinder with a conic section directrix (circle, ellipse, parabola and hyperbola). The most significant results of this consideration are listed below.

1. The diffraction corrections to the phase of backscattered fields have opposite signs for TE and TM waves: they are positive for TE waves and negative for TM waves for convex surfaces. The absolute values of these corrections are different in a general case. They are equal to each other only for the parabolic cylinder and they decrease as $\cos^3 \theta$ as incident angle θ increases. (The angle of incidence θ is counted off from the direction of the longest axis of the ellipse, or from the axis of symmetry for the parabola and hyperbola). For a circular cylinder, the phase correction to the TM wave is almost twice as much as that for the TE wave: their ratio is equal to 11/5.

2. For the elliptic cylinder, the diffraction corrections to the phase, averaged over all ellipse orientations (or over all incident angles θ), slowly depend on the ellipse semi-axis ratio r : for the TE wave they vary from $2/(3\pi p)$ for $r = 0$ (parabolic cylinder) to $5/(16p)$ for $r = 1$ (circular cylinder); for the TM wave they vary from $-2/(3\pi p)$ at $r = 0$ to $-11/(16p)$ at $r = 1$. The phase difference varies from $4/(3\pi p)$ to $1/p$ when r increases from 0 to 1. (Here, as everywhere in the text, $p = a_0 k$, where a_0 is a curvature radius at the surface apex point, i.e., the minimal curvature radius of the conic section directrix, and a_0 is assumed to be the same for all cylinders).

3. When the direction of the incident wave coincides with the conic section main axis, i.e., $\theta = 0$, the diffraction corrections are positive for HH and are negative for VV backscattering cross-sections σ_{HH} and σ_{VV} for all directrices, with the exception of hyperbola with $r > 3.1445$, which corresponds to the obtuse angles $\psi > 144.7^\circ$ between asymptotes.

4. For the elliptic cylinder, at $\theta = 0$, the minimal absolute values of corrections to the backscattering cross-sections correspond to the case $r = 1$ (circular cylinder) and maximal – to $r = 0$ (parabolic cylinder).

Normalized by p^2 , these corrections vary from $\Delta_{HH} = 19/32$ for $r = 1$ to $\Delta_{HH} = 5/4$ for $r = 0$, and from $\Delta_{VV} = -29/32$ for $r = 1$ to $\Delta_{VV} = -7/4$ for $r = 0$. At the same time, the HH/VV polarization ratio Δ_{HV} varies from $\Delta_{HV} = 3/2$ for the circular cylinder to $\Delta_{HV} = 3$ for the parabolic cylinder.

5. When θ increases, all these corrections decrease, and at some incident angles θ_0 can vanish and even change their signs. For the parabolic cylinder, Δ_{HH} changes its sign at $\theta_0 \simeq 42.4^\circ$, $\Delta_{VV} = 0$ at $\theta_0 \simeq 47.2^\circ$, and $\Delta_{HV} = 0$ at $\theta_0 = 45^\circ$.

6. At the incident angles θ , close to $\theta \simeq 23^\circ$, the diffraction corrections to the backscattering cross-sections Δ_{HH} , Δ_{VV} , as well as to the polarization ratio Δ_{HV} , are not sensitive to the value of the ellipse semi-axis ratio r , and they are almost the same for all elliptic cylinders, including the circular and the parabolic cylinders in the limiting cases $r = 1$ and $r = 0$, correspondingly. For the hyperbolic cylinders the same effect take place at smaller angles ($\theta \simeq 18^\circ$ – 20°) for $r \lesssim 1$.

7. The polarization ratio Δ_{HV} , being positive at $\theta = 0$, decreases for all type of cylinders with arbitrary conic section directrices, as θ decreases, and Δ_{HV} changes its sign in the interval of incident angles $90^\circ \geq \theta \geq 45^\circ$ for ellipses with semi-axis ratio r varying in the interval $1/\sqrt{2} \geq r \geq 0$. The polarization ratio Δ_{HV} does not change its sign, remaining positive for all incident angles for ellipses with $1 \geq r \geq 1/\sqrt{2}$.

8. For a hyperbolic cylinder, the polarization ratio Δ_{HV} changes its sign at the incident angle θ_0 , which decreases monotonically as parameter r increases from $\theta_0 = \pi/4$ for $r = 0$ (parabolic cylinder) to $\theta_0 = \pi/6$ for $r = 1$ (hyperbola with orthogonal asymptotes $\psi = \pi/2$), and θ_0 tends to zero for $r \rightarrow \infty$.

9. The diffraction corrections to the backscattering cross-sections from the hyperbolic cylinder increase $\sim r^4$ for $r \gg 1$, and tend to infinity when the incident angle θ approaches the critical angle $\theta_m = \arctan(1/r)$, i.e., when the direction of the wave propagation α (see Fig. 1) becomes orthogonal to the hyperbola asymptote. The polarization ratio Δ_{HV} increases as $\sim r^2$ for $r \gg 1$ and tends to zero at $\theta \rightarrow \theta_m$, remaining negative in the interval $\theta_m \geq \theta \geq \theta_0$.

10. From comparison of results obtained for cylinders with different conic section directrices, but with the same curvature radius a_0 at the apex point, it follows that the maximal diffraction corrections to the GO values of backscattering cross-sections and polarization ratio occur when the hyperbolic cylinder with $r \gg 1$ (and, consequently, with the very obtuse corner angle $\psi \rightarrow \pi$) is illuminated by the wave propagating along the hyperbola axis of symmetry, i.e., at $\theta = 0$.

ACKNOWLEDGMENT

Author is grateful to Dr. Mikhail Charnotskii (Zel Technologies, LLC and NOAA/Environmental Technology Laboratory, USA) and Dr. Ning Yan Zhu (Institut für Hochfrequenztechnik, Germany) for their remarks and insightful suggestions which allowed to improve the manuscript. Constructive comments by anonymous reviewers are also gratefully acknowledged.

REFERENCES

1. Morse, P. M. and H. Feshbach, *Methods of Theoretical Physics*, Part I, McGraw-Hill, New York, 1953.
2. Watson, G. N., "The diffraction of electrical waves by the earth," *Proc. Roy. Soc. (London)*, Vol. A95, 83–99, 1918.
3. Wait, J. R., *Electromagnetic Radiation from Cylindrical Structures*, Pergamon, New York, 1959.
4. Kouyoumjian, R. G., "Asymptotic high-frequency methods," *Proc. IEEE*, Vol. 53, 864–876, August 1965.
5. Bowman, J. J., T. B. A. Senior, and P. L. E. Uslenghi, *Electromagnetic and Acoustic Scattering by Simple Shapes*, Hemisphere Publishing Corp., New York, 1987.
6. Keller, J. B., R. M. Lewis, and B. D. Seckler, "Asymptotic solution of some diffraction problems," *Comm. Pure Appl. Mathem.*, Vol. 9, 207–265, 1956.
7. Keller, J. B., "Geometrical theory of diffraction," *J. Opt. Sci. Am.* Vol. 52, 116–130, 1962.
8. Babič, V. M. and V. S. Buldyrev, *Short-wavelength Diffraction Theory*, Springer-Verlag, Berlin, 1991.
9. Borovikov, V. A. and B. Ye. Kinber, *Geometrical Theory of Diffraction*, The Institution of Electrical Engineers, London, 1994.
10. Kravtsov, Yu. A. and Yu. I. Orlov, *Geometrical Optics of Inhomogeneous Media*, Springer-Verlag, Berlin, 1990.
11. Fuks, I. M., "Reflection and refraction of a wave of arbitrary shape on a curvilinear surface (in Russian)," *Izv. VUZ., Radiofizika*, Vol. 8, No. 6, 1078–1086, 1965; (English transl. in *Soviet Radiophysics*, Vol. 8, No. 6, 772–779, The Faraday Press, Inc., New York, 1965).
12. Gel'chinskii, B. Ya., "Reflection and refraction of an elastic wave of arbitrary form in the case of a curved interface," *Soviet Phys. – Doklady*, Vol. 3, No. 1, 186–188, 1958.

13. Fok, V. A., "Generalization of reflecting formulas to the case of reflection of an arbitrary wave from a surface of arbitrary shape," *Soviet Phys.-JTF*, Vol. 20, No. 11, 961–978, 1950.
14. Keller, J. B. and H. B. Keller, "Determination of reflected and transmitted fields by geometrical optics," *J. Opt. Soc. Am.*, Vol. 40, No. 1, 48–52, 1950.
15. Bass F. G. and I. M. Fuks, *Wave Scattering from Statistically Rough Surfaces* (in Russian), Nauka, Moscow, 1972; (English translation: *International Series in Natural Philosophy*, Vol. 93, C. B. Vesecky and J. F. Vesecky (eds.), Pergamon, Oxford, 1978).
16. Schensted, C. E., "Electromagnetic and acoustical scattering by a semi-infinite body of revolution," *J. Appl. Phys.*, Vol. 26, 306–308, 1955.
17. Lee, S.-W., "Electromagnetic reflection from a conducting surface: geometrical optics solution," *IEEE Trans. Antennas Propagat.*, Vol. AP-23, No. 2, 184–191, March 1975.
18. Fuks, I. M., "High-frequency asymptotic expansions of a backscattered cross-section and *HH/VV* polarization ratio for smooth two-dimensional surfaces," *Waves Random Media*, Vol. 14, 143–156, 2004.
19. West, J. C., "Low-grazing-angle (LGA) sea-spike backscattering from plunging breaker crests," *IEEE Trans. Geosci. Remote Sensing*, Vol. 40, 523–526, 2002.
20. Brekhovskikh, L. M., "Wave diffraction by a rough surface," Parts 1 and 2, *Sov. Phys. JETP*, Vol. 23, No. 3(9), 275–288, 289–304, 1952.
21. Isakovich, M. A., "Wave scattering from a statistically rough surface," *Sov. Phys. JETP*, Vol. 23, No. 3(9), 305–314, 1952.
22. Abramowitz, M. and I. A. Stegun, *Handbook of Mathematical Functions with Formulas, Graphs, and Mathematical Tables*, Dover, New York, 1972.

Iosif M. Fuks was born in June 1940, in Kharkov, Ukraine. He received the MS degree in theoretical physics from the University of Kharkov in 1962 and joined the Institute of Radio Physics and Electronics Ukrainian Academy of Sciences. In 1966, from the Acoustics Institute of Academy of Sciences of the USSR (Moscow), he obtained the Candidate of Science (Ph.D.) degree on the theory of radio waves scattering by statistically rough surfaces. In 1978 he received the Doctor of Science (Physics and Mathematics) degree from the University of Kharkov and became a full professor of space radio

physics at Kharkov University. In 1987 he obtained the Ukrainian National Science and Technology Prize. In 1980, he joined the Institute of Radio Astronomy of the Ukrainian National Academy of Sciences in Kharkov, where he has been a head of the Space Radio Physics Laboratory since 1985. Since 1997 he has been working for NOAA Environmental Technology Laboratories at Boulder, Colorado. He has co-authored more than 150 papers, covering different aspects of wave propagation and diffraction theory. Professor Fuks's research interests lie in the statistical theory of diffraction on rough surfaces and wave propagation through random media, thermal electromagnetic emission from natural objects, analytical and numerical simulation methods for solving diffraction, and radio wave propagation problems.